COMMUNICATIONS PHYSICS

ARTICLE

https://doi.org/10.1038/s42005-019-0117-9 OPEN

Poly-stable energy harvesting based on synergetic multistable vibration

Huaxia Deng [1], Yu Du [1], Zhemin Wang[1], Jingchang Ye[1], Jin Zhang[1], Mengchao Ma[1] & Xiang Zhong[1]

Distributed energy sources, for example the ambient broadband vibrations, are of great importance for the development of the Internet of Things. However, for multistable vibrational energy harvesters, increasing the number of stable equilibrium states to broaden working frequency bands is very difficult. Here we present a poly-stable vibrational energy harvesting approach capable of achieving an exponentially growing maximum number of stable equilibrium states. Unlike the traditional multistable harvesters relying on an external static magnetic field, the nonlinear dynamical behaviours achieved by the proposed approach are synergetic poly-stable motions without the need of external magnets. Comparison experiments in contrast with a linear harvester demonstrate the working bandwidth widened by a factor of 41.0, the power density increased to 760% and the electricity generation raised to 178%. This demonstration of new multistable energy harvester expands the approach to achieving multistable motion and provides a new design philosophy for nonlinear vibrational energy harvesters.

[1] School of Instrument Science and Opto-electronics Engineering, Hefei University of Technology, Hefei, Anhui 230009, People's Republic of China. These authors contributed equally: Huaxia Deng, Yu Du, Zhemin Wang. Correspondence and requests for materials should be addressed to H.D. (email: hxdeng@hfut.edu.cn)

Vibrational motion, as one of the most widespread renewable energy sources, exists in a variety of forms in natural environments, examples being ocean waves[1–6], vibrations of machinery[7–9], and motions of the human body[10–15]. To convert this vibrational energy into electricity for utilization in self-powered sensor networks[16] and other low-power electronic devices, a variety of energy harvesters have been proposed[17–22]. Most existing vibrational energy harvesters are based on a resonance principle and work mainly near structural resonant frequencies[23,24]. Ambient vibrational excitations are random and of low frequency and low intensity[25,26]. To harvest vibrational energy over a wide-frequency range[27], nonlinear energy harvesters have been proposed to broaden the working frequency bands.

Nonlinear energy harvesters[28,29], typically relying on multistable motions of a beam or plate[30,31], are capable of achieving wide-working bandwidths[26,32–34]. The principle of using multistable motions to broaden working bandwidths is that dynamic behavior, reflected directly in the amplitudes of vibration, is improved at nonresonant frequencies. Early nonlinear energy harvesters relied on a magnetically coupled cantilever beam or a buckled beam[23,35,36] to achieve bistable motions. A bistable piezoelectric energy harvester, employing the magnetic attractions between the tip magnet of a cantilever beam and two external magnets to realize bistable motion, generates greater output power than the corresponding linear device over a wide-frequency range[23]. Subsequently, magnetic-repulsion-type bistable energy harvesters have been developed, using a single external magnet to provide magnetic repulsion[37–39]. The potential energy of a bistable system has two potential wells, one on each side of a potential barrier[40]. Achieving bistable motion (inter-well motion) requires that sufficient energy be provided by external excitations to overcome the potential barrier[37].

Taking bistable energy harvesters as a basis, by adjusting the spacing between the magnets[40], changing the magnet inclination angles[41], or increasing the number of external magnets[42], multistable energy harvesters, such as tri-stable[34,42] and even quad-stable[43,44] harvesters, have been proposed. Theoretical and experimental studies of multistable energy harvesters show that increasing the number of stable equilibrium states contributes to broadening the working frequency bands while harvesting energy from low-intensity vibrational sources[45,46]. A quad-stable energy harvester utilizing magnetic repulsion by three external magnets, with lower potential barriers than those of the corresponding bistable device, exhibits a wider working bandwidth because of the lower excitation energy required to escape from the potential wells[43]. Despite all of these efforts, with existing multistable energy harvesters in which external magnets are used to provide magnetic forces, it is very difficult to achieve five or more stable equilibrium states because of limitations imposed by their mechanism of motion[44]. To further improve the dynamic responses of multistable harvesters and enhance their generation efficiency under broadband vibrational excitation, it is necessary to increase the number of stable equilibrium states.

This paper finds an interesting phenomenon named synergetic poly-stable nonlinear motion, in which the maximum number of stable equilibrium states has an exponential dependence on the number of interacting masses. To research the potential energy of a synergetic poly-stable beam array, the magnetic interactions among different beams are analyzed by using the magnetic dipole model. The stable equilibrium states are calculated and enumerated to demonstrate the poly-stability of the beam arrays. Using the synergetic poly-stable beam arrays, a kind of composable vibrational energy harvesting brick is developed to collect broadband multidirectional vibrational energy. Electricity generation experiments comparing the poly-stable beam array with a linear beam array verify the condition of realizing poly-stable motion and its broadband characteristics.

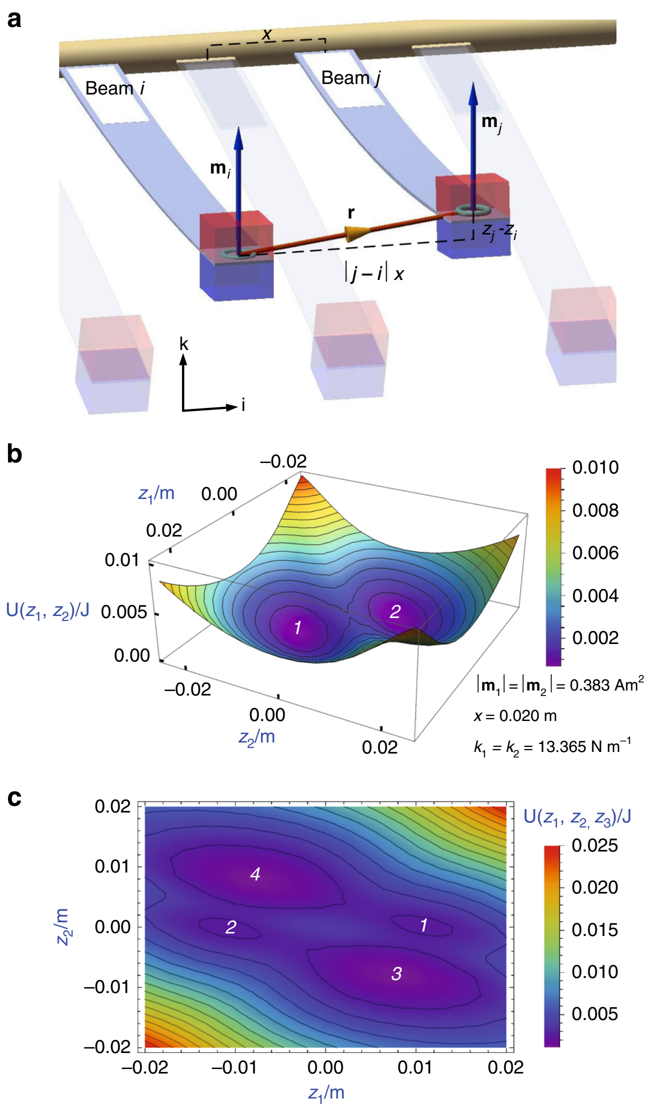

Fig. 1 Magnetic interactions and potential energy. **a** Magnetic interactions between different beams. **b** Potential energy of a double-beam SPBA (synergetic poly-stable beam array). **c** Potential energy of a triple-beam SPBA

Results

Mechanism. The proposed poly-stable energy harvesting method is implemented via a synergetic poly-stable beam array (SPBA). An SPBA comprises several cantilever beams placed side by side, with mutually repelling magnets at their tips. In order to research the poly-stable energy harvesting mechanism and realizing conditions of the synergetic poly-stable motion, the potential energy of the SPBA is analyzed to reveal the relationship between displacements of the beams and stable equilibrium states of the SPBA. The magnetic interactions between different beams are analyzed by using the magnetic dipole model. As shown in Fig. 1a, in a SPBA composed of n cantilever beams, magnetic dipole i and j represent the equivalent points of the two tip magnets of cantilever beam i and j, respectively ($i, j \in \{1, 2, \ldots, n\}$, $i \neq j$). In the SPBA, the horizontal spacing between any two adjacent beams is x, therefore the horizontal spacing between beam i and beam j is $|j-i|x$. The displacements of the beam i and beam j are denoted by z_i and z_j, respectively.

With the magnetic moments of magnetic dipole i and j denoted by $\mathbf{m}_i$ and $\mathbf{m}_j$ respectively, the magnetic flux density produced by magnetic dipole i at magnetic dipole j can be expressed as

$$\mathbf{B}_{ij} = -\frac{\mu_0}{4\pi}\nabla\frac{\mathbf{m}_i\cdot\mathbf{r}}{|\mathbf{r}|^3}, \quad (1)$$

where $\mu_0 = 4\pi\times10^{-7}\ \mathrm{H{\cdot}m^{-1}}$ is the permeability of vacuum, $\nabla = \frac{\partial}{\partial_x}\mathbf{i} + \frac{\partial}{\partial_z}\mathbf{k}$ is vector differential operator. $\mathbf{i}$ and $\mathbf{k}$ are the unit vector of horizontal direction and vertical direction, respectively. $\mathbf{r}$ is the direction vector from magnetic dipole i to magnetic dipole j. Ignoring the rotation angles of the beams at the free ends, the magnetic potential energy between the two beams[47] can be expressed as

$$U_{ij} = -\mathbf{B}_{ij}\cdot\mathbf{m}_j = \frac{\mu_0|\mathbf{m}_i|\left|\mathbf{m}_j\right|\left[(j-i)^2x^2 - 2\left(z_j-z_i\right)^2\right]}{4\pi\left[(j-i)^2x^2 + \left(z_j-z_i\right)^2\right]^{\frac{5}{2}}}. \quad (2)$$

The elastic potential energy of cantilever beam i is

$$U_i = \frac{1}{2}k_i z_i^2, \quad (3)$$

where k_i is the stiffness of cantilever beam i. Then the total magnetic potential energy $U_\mathrm{m}(z_1, z_2, \ldots, z_\mathrm{n})$ and the total elastic potential energy $U_\mathrm{e}(z_1, z_2, \ldots, z_\mathrm{n})$ can be expressed as

$$\begin{aligned} U_\mathrm{m}(z_1,z_2,\cdots,z_\mathrm{n}) &= \tfrac{1}{2}\sum_{i,j=1(i\neq j)}^{\mathrm{n}} U_{ij} \\ &= \sum_{i,j=1(i\neq j)}^{\mathrm{n}} \frac{\mu_0|\mathbf{m}_i|\left|\mathbf{m}_j\right|\left[(j-i)^2x^2-2\left(z_j-z_i\right)^2\right]}{8\pi\left[(j-i)^2x^2+\left(z_j-z_i\right)^2\right]^{\frac{5}{2}}}, \end{aligned} \quad (4)$$

$$U_\mathrm{e}(z_1,z_2,\cdots,z_\mathrm{n}) = \sum_{i=1}^{\mathrm{n}} U_i = \frac{1}{2}\sum_{i=1}^{\mathrm{n}} k_i z_i^2. \quad (5)$$

The total potential energy

$$U(z_1,z_2,\cdots,z_\mathrm{n}) = U_\mathrm{m}(z_1,z_2,\cdots,z_\mathrm{n}) + U_\mathrm{e}(z_1,z_2,\cdots,z_\mathrm{n}). \quad (6)$$

To illustrate the poly-stability of the SPBA, the total potential energies of a double-beam SPBA and a triple-beam SPBA are presented in Fig. 1b, c, respectively. Since the ternary function cannot be expressed in the coordinate system, Fig. 1c presents the potential energy distribution within the spatial plane $5z_1 + 8z_2 + 5z_3 = 0$, which can also reflect the poly-stability of a triple-beam SPBA.

According to the principle of minimum potential energy, a system is in a stable equilibrium state when its potential energy reaches to a local minimum value. The stable equilibrium conditions can be described as

$$\begin{cases} \frac{\partial U(z_1,z_2,\cdots,z_\mathrm{n})}{\partial z_1} = \frac{\partial U(z_1,z_2,\cdots,z_\mathrm{n})}{\partial z_2} = \cdots \\ \qquad = \frac{\partial U(z_1,z_2,\cdots,z_\mathrm{n})}{\partial z_\mathrm{n}} = 0 \\ \frac{\partial^2 U(z_1,z_2,\cdots,z_\mathrm{n})}{\partial z_i^2} > 0, i = 1,2,\cdots,\mathrm{n}. \end{cases} \quad (7)$$

Obviously, the potential energy $U(z_1, z_2)$ in Fig. 1b has two local minimum values corresponding to the two stable equilibrium states, $(z_1, z_2) = (7.1, -7.1)$ or $(-7.1, 7.1)$ mm, which proves that an SPBA comprising of two cantilever beams is a bistable system. For a triple-beam SPBA, the potential energy $U(z_1, z_2, z_3)$ in

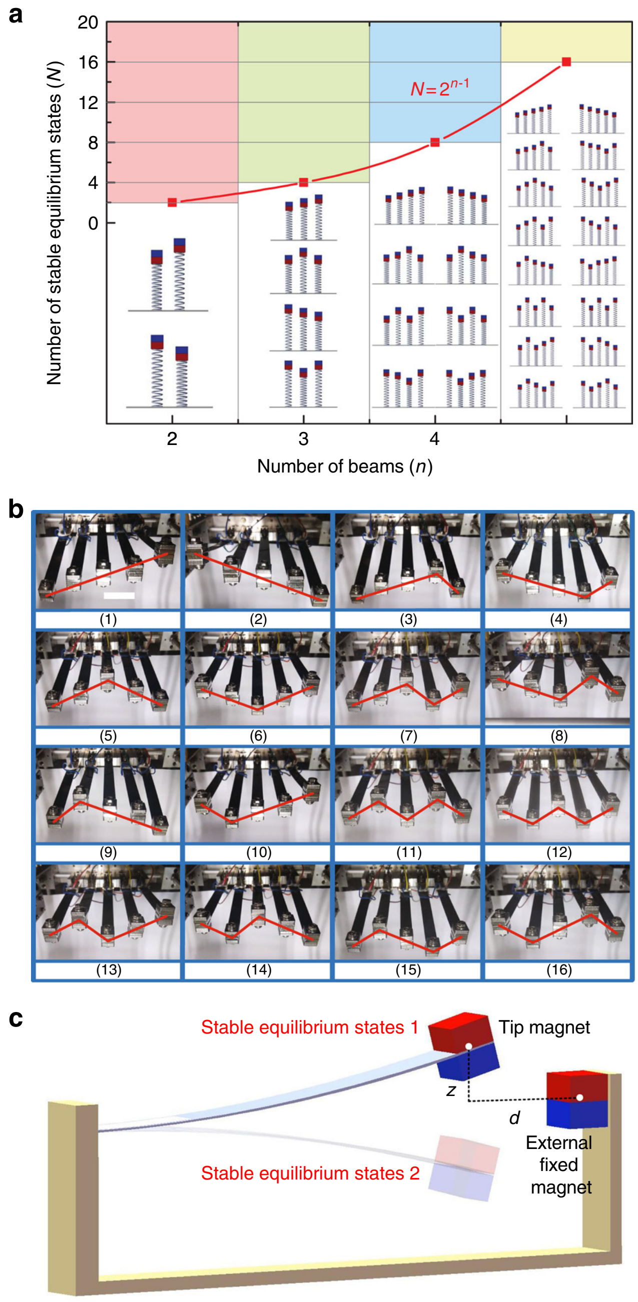

Fig. 2 Enumeration of the stable equilibrium states. **a** SPBAs (synergetic poly-stable beam arrays) with different number of beams. **b** The photographs of sixteen stable equilibrium states of a quintuple-beam SPBA. Scale bar is 20 mm. **c** A traditional multistable harvester

Fig. 1c exhibits four local minimum values, which corresponds to a quad-stable system ($(z_1, z_2, z_3) = (11.2, 0, -11.2)$, $(-11.2, 0, 11.2)$, $(5.3, -10.5, 5.3)$, or $(-5.3, 10.5, -5.3)$ mm). On the basis of the stable equilibrium conditions, all the stable equilibrium states of an SPBA are enumerated in Fig. 2a, where the cantilever beams are simply represented by spring-mass models. Figure 2b presents the photographs of sixteen stable equilibrium states of an SPBA consisting of five beams.

As shown in Fig. 2a, the more cantilever beams there are, the more stable equilibrium states the SPBA has. The five-beam SPBA in Fig. 2b has a maximum of sixteen stable equilibrium states, examples being V shape (Photograph 6), M shape (Photograph 11), and W shape (Photograph 12). It can be

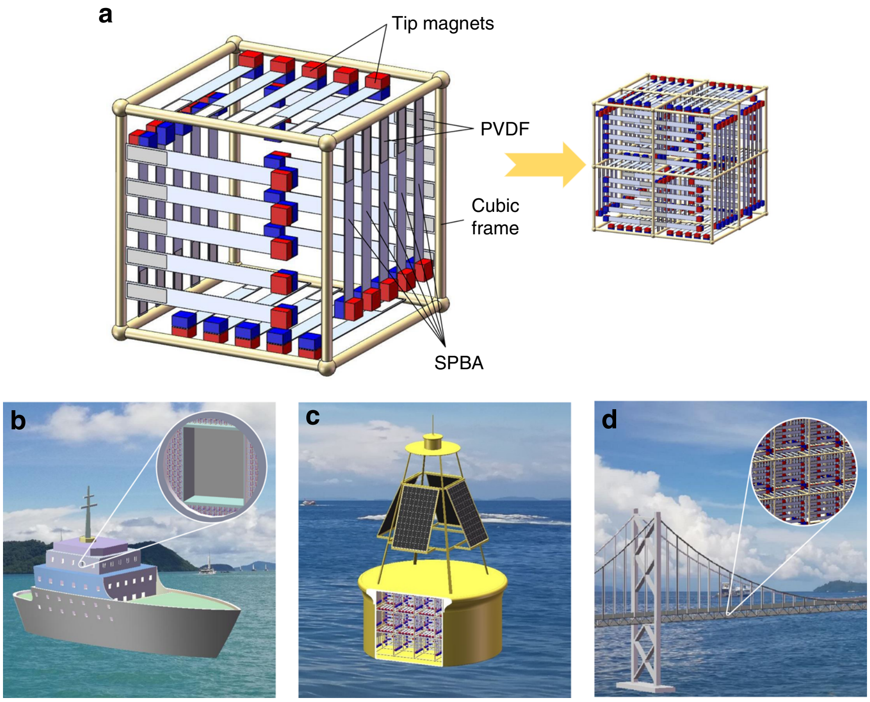

Fig. 3 The proposed energy harvesting brick and some of its applications: **a** the energy-harvesting brick incorporating SPBAs (synergetic poly-stable beam arrays) and PVDF (polyvinylidene fluoride) piezoelectric films; **b** energy-harvesting bricks used to make a non-load-bearing wall in a ship; **c** energy-harvesting bricks installed in an ocean buoy; **d** energy-harvesting bricks installed under a bridge

further concluded that an SPBA composed of n cantilever beams has a maximum of 2^{n-1} stable equilibrium states, although the actual number is limited by the stiffnesses k_i of the beams and the horizontal spacing x between them. The maximum number of stable equilibrium states of the SPBA increases exponentially with the number of beams, which is beneficial for broadening the working frequency bands.

Compared with a traditional multistable harvester, as shown in Fig. 2c, both the mechanisms and the stable equilibrium states of the proposed SPBA are different. In terms of mechanisms, the traditional independent multistable harvester relies on an external static magnetic field provided by the external fixed magnet, while the beams of the SPBA interact with each other through the dynamic magnetic fields that they themselves generate. The differentia of mechanisms can be further illustrated by comparing their potential energy functions. The magnetic potential energy of the traditional multistable harvester is presented in expression 8,

$$U_{\mathrm{Trad}}(z) = \frac{\mu_0|\mathbf{m}_{\mathrm{T}}||\mathbf{m}_{\mathrm{E}}|(d^2 - 2z^2)}{4\pi(d^2 + z^2)^{\frac{5}{2}}} \tag{8}$$

$$U_{\mathrm{m}}(z_1, z_2, \cdots, z_{\mathrm{n}}) = \sum_{i,j=1(i\neq j)}^{\mathrm{n}} \frac{\mu_0|\mathbf{m}_i||\mathbf{m}_j|\left[(j-i)^2x^2 - 2\left(z_j - z_i\right)^2\right]}{8\pi\left[(j-i)^2x^2 + \left(z_j - z_i\right)^2\right]^{\frac{5}{2}}} \tag{9}$$

which is a univariate function depending totally on the absolute displacement z of the beam when the structural parameters (the horizontal spacing d between the tip magnet and the external fixed magnet, the magnetic moment $\mathbf{m}_{\mathrm{T}}$ of the tip magnet, and the magnetic moment $\mathbf{m}_{\mathrm{E}}$ of the external fixed magnet) are constant. The magnetic potential energy $U_{\mathrm{m}}(z_1, z_2, \ldots, z_{\mathrm{n}})$, as a multivariate function, intuitively demonstrates that the magnetic potential energy of the SPBA depends on the relative displacements $z_j - z_i$ between different beams instead of absolute displacements. Corresponding to the local minimum values of potential energy, the stable equilibrium states of a traditional multistable harvester manifest as achieving stable equilibria at several different displacements, as shown in Fig. 2c, while the stable equilibrium states of the SPBA mainly reflect in the multiple stable relative location relations of different beams, as enumerated in Fig. 2b.

The different mechanisms lead to the different forms of stable equilibrium states, which further lead to a different multistable motion. The traditional multistable motion manifests as a reciprocating motion spanning multiple stable equilibrium positions of a single beam, while the synergetic poly-stable motion of the SPBA is reflected in the change of relative positions of different beams—from one stable spatial location-relation to another. In addition, the potential energy expression of the SPBA also reveals the condition of realizing the synergetic poly-stable motion: the relative displacements $z_j - z_i$ between different beams have to be variable. If all the relative displacements are constant, the magnetic potential energy $U_{\mathrm{m}}(z_1, z_2, \ldots, z_{\mathrm{n}})$ will become a constant value. Accordingly, the total potential energy $U(z_1, z_2, \ldots, z_{\mathrm{n}})$ becomes a univariate quadratic function, which corresponds to a monostable system. Therefore, the beams in the SPBA should have different natural frequencies so as to have different responses under the same external excitations.

Applications. On the basis of the SPBA, a vibrational energy harvesting brick is desigened, which is not only composable but also able to achieve multidirectional vibrational energy harvesting over a wide-frequency range. The energy harvesting brick makes use of six SPBAs, as shown in Fig. 3a. An SPBA is installed in each face of a cubic frame to collect multidirectional vibrational energy. The beams in each SPBA have different thicknesses as well as different natural frequencies. As a composable structural unit, the cubic brick is like a cell that can be integrated into other engineering structures, such as non-load-bearing architectural constructions, without taking up otherwise useful space. Therefore, the energy harvesting bricks can be used in engineering field

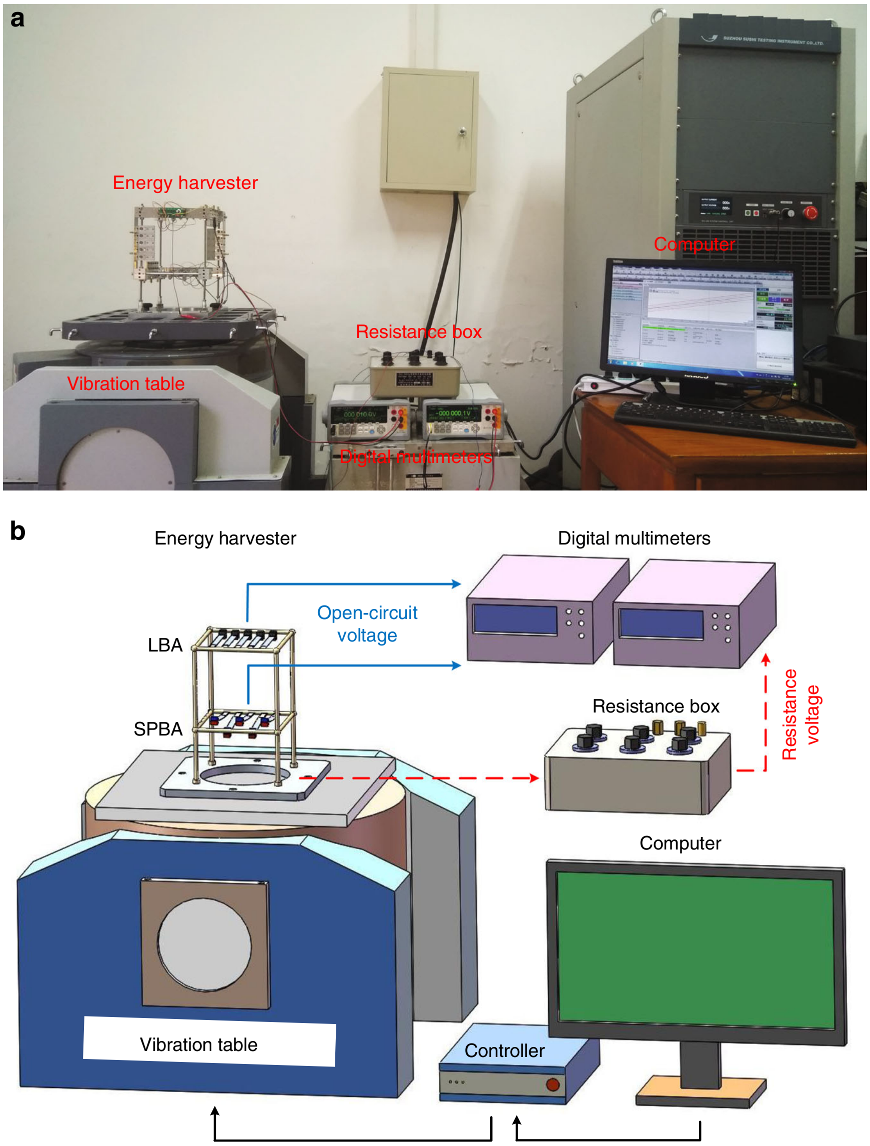

Fig. 4 Experimental setup. **a** Photograph. **b** Schematic diagram (LBA and SPBA represent linear beam array and synergetic poly-stable beam array, respectively)

on a large scale to achieve high-power generation without the need of considering limitations of space and volume.

As shown in Fig. 3b, by constructing a non-load-bearing wall with the proposed energy harvesting bricks, without changing the structure of the hull, the vibrational energy of a ship can be collected in real time and supplied to electrical systems, thereby reducing consumption of fossil energy. Figure 3c shows how the floating body of an ocean buoy can be filled with energy-harvesting bricks, from which the buoy can supplement its normal energy supply at night, in particular in polar seas, where solar energy is scarce. Energy-harvesting bricks can also be combined with other architectural constructions, such as the bridge shown in Fig. 3d. Under the dynamic loads produced by moving vehicles, vibration of the bridge is unavoidable, and the vibrational energy can be harvested and converted by the bricks to supply electrical power for a network of sensors monitoring the structural health of the bridge.

Experimental setup. In order to verify the theoretical conclusions and study the broadband characteristics as well as the improvements in generation efficiency brought about by the synergetic poly-stable motion of the proposed SPBA, the following electricity-generation experiments are set up, where a linear beam array (LBA) consisting of five beams with different natural frequencies is used as a comparison. As shown in Fig. 4, the LBA is fixed at the top of the cubic frame and the SPBA is fixed at the bottom. All the tip mass blocks of the five beams in the LBA are nonmagnetic and have the same mass as that of the SPBA. The vibration table provides swept excitations for the energy harvester from 3 to 23 Hz to simulate the ambient low-frequency excitation with low intensity. The sweep rate is 0.2 Hz per second, and the excitation amplitude $A = 2$ mm. Two digital multimeters are used to record the output voltages, and a resistance box is used as the external load. The experimental setup is shown in Fig. 4.

SPBA composed of single-frequency beams. The theoretical analyses demonstrate that the SPBA will become a monostable system if all the relative displacements between different beams are constant. To verify this conclusion, an SPBA composed of five single-frequency beams is compared with a corresponding linear beam in the LBA. All the six beams in this experiment have the

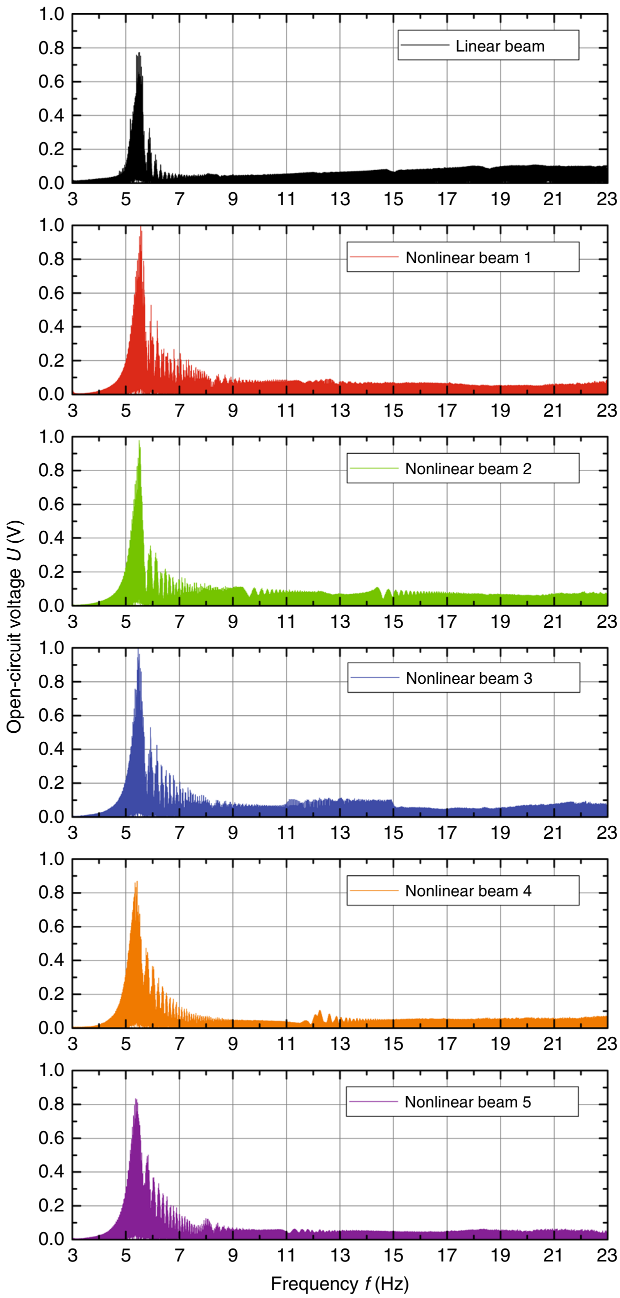

Fig. 5 Open-circuit voltages of the five nonlinear beams in the SPBA (synergetic poly-stable beam array) and the corresponding linear beam

same thicknesses (0.3 mm) as well as natural frequencies. The open-circuit voltages of the six beams are plotted in Fig. 5 to research their responses under the same swept excitations.

As shown in Fig. 5, during the entire sweep process, the open-circuit voltages of the five nonlinear beams in the SPBA are all similar to that of the corresponding linear beam in the LBA. When the excitation frequency reaches about 5.5 Hz, the nonlinear beams and the corresponding linear beam resonate simultaneously so that their output voltages reach peek values at the same time. After the resonances, the output voltages of both the nonlinear beams and the linear beam start to decline rapidly, which do not exceed 0.1 V from 9 to 23 Hz.

Due to the same thicknesses as well as natural frequencies, all the beams in the SPBA have the same responses under the same excitations (see Supplementary Movie 1). Although the five beams repel each other via their tip magnets, the same responses lead to the constant relative displacements, which further result in a stable relative location-relation of the five beams with an M shape (Photograph 11 in Fig. 2b). The five nonlinear beams in the SPBA keep synchronous motions with almost the same amplitudes and phases during the entire sweep process. In such situation, the output of each beam in the SPBA certainly cannot exhibit noticeable improvement. These experimental phenomena prove that the SPBA, with the constant relative displacements, becomes a monostable system that cannot achieve synergetic poly-stable motion, which is in agreement with the result of theoretical analyses.

SPBA composed of multi-frequency beams. To achieve synergetic poly-stable motion, the SPBA composed of five beams with different thicknesses as well as natural frequencies is used in the following experiment so as to ensure the relative location-relations of the beams be variable. The thicknesses of the five beams in the SPBA are corresponding to that of the LBA.

Under the same swept excitations, the open-circuit voltage of each beam is recorded and depicted in Fig. 6 to allow study of the broadening of the working band. Taking the forward voltage drop (0.5 V) of the common rectifier bridges as the minimum effective output voltage of the energy harvester, the effective working bands of the SPBA and LBA are indicated in yellow. As shown in Fig. 6a, all the working bands of the five beams in the LBA are around the resonant frequencies, because the open-circuit voltage under nonresonant frequencies barely exceeds 0.5 V. In contrast, as shown in Fig. 6b, the working bands of the five beams in the SPBA are significantly broadened and are no longer confined around the resonant frequencies of the beams. For example, in the LBA, the working band of the 0.3-mm-thick beam, from 5.34 to 5.62 Hz, is near the resonant frequency (5.50 Hz) of the beam, while in the SPBA, the working bands of the corresponding beam of the same thickness are from 6.41 to 7.33 Hz as well as from 12.43 to 23.00 Hz, which together are 41.0 times as wide as that of the LBA. The working bandwidths of the other four beams in the SPBA, from 0.4- to 0.7-mm thick, are increased to 1185, 152, 148, and 208%, respectively. This broadening of the working frequency bands of each beam in the SPBA shows the advantage of the synergetic poly-stable motion in broadband vibrational energy harvesting.

Benefiting greatly from the synergetic poly-stable motion, the five beams in the SPBA are able to drive each other in the process of vibration. During the entire sweep process, all five cantilever beams in the SPBA are clearly vibrating all the time, while in the LBA, only one beam near the resonant frequency exhibits obvious vibration (see Supplementary Movie 2). The relative location-relations of the five beams keep switching between multiple stable equilibrium states, such as the M shape, W shape, V shape, etc., as has been enumerated in Fig. 2b, even at nonresonant frequencies. These experimental phenomena reveal the reason for the increase in voltage at nonresonant frequencies. By virtue of the synergetic poly-stable motion, the SPBA exhibits broadband characteristic.

The broadening of the working band is reflected not only in the output voltage of the energy harvester, but also in its power density. To verify the effect of the synergetic poly-stable motion of the SPBA on power density, the SPBA and the LBA are compared under the same swept excitation as before. A resistance box is used as the external load, the power of which is calculated as $P = U^2/R$, where the voltage U is that recorded by the digital multimeter. According to the principle of impedance matching, 10 MΩ is taken as the load resistance. The power densities (output power per unit volume) of the SPBA and the LBA are presented in Fig. 7a. The frequency bands shaded in pink are those in which the power density of the SPBA is higher than that

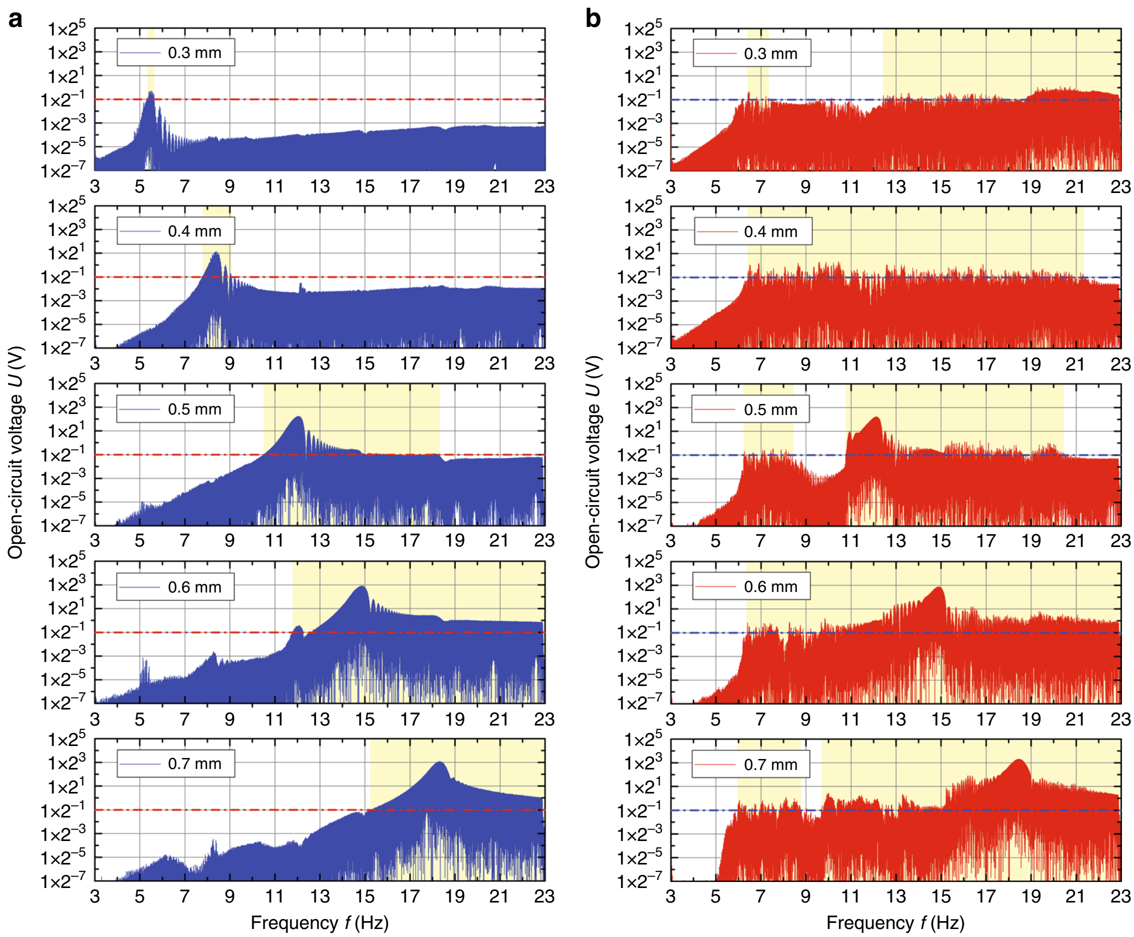

Fig. 6 Open-circuit voltages of each beam (the thickness of each beam is given in the corresponding legend): **a** in the LBA (linear beam array); **b** in the SPBA (synergetic poly-stable beam array)

of the LBA, while the cyan-shaded bands are those where the power density of the SPBA is lower than that of the LBA.

As can be seen from Fig. 7a, the power density of the SPBA is generally higher than that of the LBA except in the resonant frequency bands of the five beams, where their power densities are similar. For an energy harvester, the broadening of the working bandwidth is mainly reflected in an increase in output voltage or power at nonresonant frequencies. For instance, between the five resonant frequencies of the beams, under excitation at 7, 10, 13, and 16 Hz, the maximum instantaneous power densities of the SPBA are 1.49×10^{-1}, 1.46×10^{-1}, 7.85×10^{-1}, and 1.09 mW·m^{-3}, respectively. Thus, in comparison with the LBA, with corresponding values of 1.96×10^{-2}, 4.04×10^{-2}, 2.06×10^{-1}, and 3.58×10^{-1} mW·m^{-3}, the maximum instantaneous power densities of the SPBA are increased to 760, 361, 381, and 304%, respectively. These results clearly illustrate that the synergetic poly-stable motion of the SPBA significantly increases the power densities as a result of the interactions between the cantilever beams, especially at nonresonant frequencies. The corresponding average power densities at different frequencies are listed in Table 1, providing a clearer numerical comparison of the SPBA and the LBA.

The average power densities show a similar trend with changing excitation frequency, as shown in Table 1. The average power densities of the SPBA at nonresonant frequencies are also much larger than those of the LBA. Under excitation frequencies of 7, 10, 13, and 17 Hz, the average power densities of the SPBA are, respectively, 595, 376, 195, and 142% of that of the LBA. It is worth recalling that the transducers used here are polyvinylidene fluoride (PVDF) piezoelectric films. When these transducers are replaced by triboelectric material, the output power of the SPBA is further increased such that it becomes capable of lighting up five series-connected LEDs (see Supplementary Movie 3). The five LEDs keep glowing and flashing within a wide-frequency range, even at nonresonant frequencies, which demonstrates that this system meets the power requirements of practical applications. Moreover, the increased power under nonresonant excitation and the wider working bandwidth have the potential to enhance the generation efficiency.

To verify the enhancement of the generation efficiency, the charging rates of the capacitors are compared experimentally as follows. The sweep condition remains unchanged, while the output of each beam in the SPBA is rectified and then connected in parallel to both ends of a capacitor. During charging, the voltage U of the capacitor is recorded by a digital multimeter. For comparison, the electrical energy output of the LBA is stored in an identical capacitor under the same conditions. The electric field energies ($W = CU^2/2$) stored in the capacitors are plotted in Fig. 7b.

During the entire sweep process, the energy stored in the capacitor connected with the SPBA is almost always higher than that of the LBA. The greater slope of the charging curve of the SPBA indicates a faster charging rate as well as a higher output power. After 100 s of swept excitation, the energy harvested by the SPBA is 0.48 μJ, whereas that of the LBA is only 0.27 μJ. By virtue of the synergetic poly-stable motion of the SPBA, the

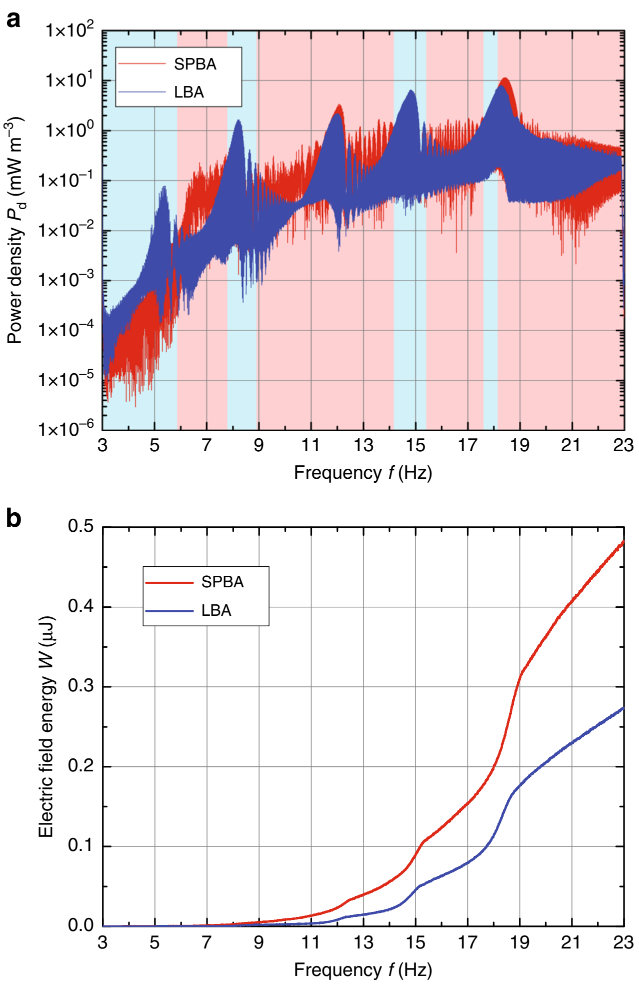

Fig. 7 Output power densities and harvested energy of the SPBA (synergetic poly-stable beam array) and the LBA (linear beam array). **a** Output power densities. **b** Electric field energies stored in the capacitors

Table 1 Average power densities (mW·m^{-3}) of the SPBA (synergetic poly-stable beam array) and the LBA (linear beam array) at different frequencies

Frequency f (Hz)	SPBA P_{d1}	LBA P_{d2}	Ratio P_{d1}/P_{d2}
3	1.48×10^{-3}	7.07×10^{-3}	21%
4	1.16×10^{-4}	3.30×10^{-4}	35%
5	6.44×10^{-4}	7.08×10^{-3}	9%
6	4.91×10^{-3}	4.15×10^{-3}	118%
7	4.92×10^{-2}	8.28×10^{-3}	595%
8	2.12×10^{-1}	3.34×10^{-1}	63%
9	8.23×10^{-2}	3.06×10^{-2}	269%
10	9.33×10^{-2}	2.48×10^{-2}	376%
11	1.69×10^{-1}	6.87×10^{-2}	246%
12	$1.48 \times 10^{+0}$	$1.05 \times 10^{+0}$	141%
13	2.12×10^{-1}	1.09×10^{-1}	195%
14	5.69×10^{-1}	3.08×10^{-1}	185%
15	$2.04 \times 10^{+0}$	$1.99 \times 10^{+0}$	103%
16	2.73×10^{-1}	2.11×10^{-1}	129%
17	4.54×10^{-1}	3.20×10^{-1}	142%
18	$2.43 \times 10^{+0}$	$2.60 \times 10^{+0}$	93%
19	5.98×10^{-1}	6.97×10^{-1}	86%
20	3.45×10^{-1}	3.47×10^{-1}	99%
21	2.83×10^{-1}	2.72×10^{-1}	104%
22	2.74×10^{-1}	2.35×10^{-1}	116%
23	2.12×10^{-1}	2.19×10^{-1}	97%

electricity generation is raised to 178%. The proposed SPBA, without increasing the number of beams, not only broadens the working bandwidth, but also improves the generation efficiency significantly.

Discussion

The proposed poly-stable vibrational energy harvesting method represents a novel approach to increasing the number of stable equilibrium states. The motion of the beam array used in this approach exhibits a novel physical phenomenon, namely, synergetic poly-stable motion. The mechanism of this motion is different from that in traditional multistable energy harvesters, which rely on an external static magnetic field to achieve stable equilibria at several fixed positions. The beams of the SPBA interact with each other through the dynamic magnetic fields that they themselves generate, and the stable equilibrium states correspond to different relative positions of the beams, such as the M, W, and V shapes in Fig. 2b. The maximum number of stable equilibrium states increases exponentially with the number of beams in the SPBA, in contrast to traditional multistable harvesters, where it is difficult for the number of such states to exceed four.

In contrast to traditional multistable harvesters, in the proposed approach, in order to increase the number of stable equilibrium states, it is not necessary to make adjustments to structural parameters such as the spacing between the magnets, the inclination angles of external magnets, or the number of external magnets, and, indeed, external magnets are not even necessary. The SPBA, relying only on the interactions between different beams to achieve synergetic poly-stable motion, exhibits novel nonlinear dynamical characteristics. On the basis of this design philosophy, it should be possible to develop a variety of poly-stable energy harvesters to collect energy from ambient broadband low-intensity vibrational sources. Moreover, the proposed poly-stable vibrational energy harvesting method is not only suitable for piezoelectric energy conversion, but also applicable to electromagnetic power generation. In combination with the use of triboelectric material, it can act as a nonlinear poly-stable triboelectric nanogenerator (NP-TENG) with high-power generation efficiency.

Comparison of experimental results for single-frequency and multi-frequency SPBAs confirms the existence of a necessary structural condition for achieving synergetic poly-stable motion, namely, that the beams in the SPBA should have different natural frequencies. It should be noted, however, that this condition does not limit the applications of the proposed method. Conversely, dynamic coupling of multi-frequency beams is beneficial in widening the working frequency bands and improving the energy harvesting efficiency. There are a number of aspects of the proposed poly-stable energy harvesting method that deserve investigation in future work. For example, changes in structural parameters, such as the spacing between any two adjacent beams, the number of beams, and the sequences of beams with different natural frequencies in the array, are likely to affect the poly-stability of the SPBA.

By virtue of the synergetic poly-stable motion, the energy-harvesting performance is significantly improved in terms of open-circuit voltage, power density, working bandwidth, and generation efficiency. If an SPBA is installed into each face of an energy-harvesting brick, such a brick will be capable of harvesting multidirectional broadband vibrational energy. Without the need for external magnets, the structure of an energy harvester can become more compact, and it is then more convenient to enhance power generation by increasing the number of cantilever beams. Different structural designs will enable SPBAs to be applied to a variety of energy harvesters to collect multidirectional broadband vibrational energy in a range of natural environments.

In conclusion, in this paper we propose a different approach to achieve multistable vibrational energy harvesting based on synergetic poly-stable nonlinear motions. Potential energy analyses reveal that the mechanism of these nonlinear motions is based on interactions among dynamic magnetic masses rather than the static external magnetic fields of traditional multistable harvesters. The maximum number of stable equilibrium states theoretically increases exponentially with the number of magnetic masses. Experiments comparing electricity generation by a poly-stable harvester and a corresponding linear harvester show that synergetic poly-stable motion is achieved when the beams in the SPBA have different natural frequencies. This synergetic poly-stable motion significantly improves electricity generation performance, especially at nonresonant frequencies. Notably, the working band is broadened by a factor of 41.0 and the power density is increased to 760%. With the proposed SPBA, the electricity generation is increased to 178%. Based on the proposed approach, a composable energy-harvesting brick is designed, which can be used as a structural unit in engineering structures, such as non-load-bearing walls, without taking up otherwise useful space. Poly-stable energy harvesting thus provides a promising approach to achieving multistable motion and opens up many new possibilities for environmental energy harvesters.

Methods

Arrangement of the experimental device. All the cantilever beams are made of 65 Mn spring steel with the dimension of $105.0 \times 10.0\ \mathrm{mm}^2$. The cantilever beams in the arrays are arranged in order of thickness from thin to thick. The magnetization of the tip magnets is $1275\ \mathrm{kA{\cdot}m^{-1}}$. All the tip magnets and tip mass blocks have the same mass 10.0 g. All the beams are coated with PVDF (polyvinylidene fluoride) piezoelectric films at their fixed ends. The area of each PVDF film is $15.0 \times 10.0\ \mathrm{mm}^2$.

Measurements of the experimental data. All the voltage data are recorded by two digital multimeters (ZLG DMM6000 and ZLG DMM6001). In the power experiments, 10 MΩ is taken as the load resistance, and the output power is calculated using the formula $P = U^2/R$. The capacitors used in the experiment have the same capacitance, 470 μF, and the electric field energies stored in the capacitors are calculated using the formula $W = CU^2/2$. In this paper, all the experimental data are outputs of the PVDF piezoelectric films, while in Supplementary Movie 3, in order to enhance the output voltages and powers to light up five LEDs, transducers on the fixed ends of the cantilever beams are replaced by triboelectric material. The output of each beam is rectified and then connected in parallel to the five series-connected LEDs.

Data availability

The data that support the findings of this study are available from the corresponding author upon reasonable request.

Received: 24 August 2018 Accepted: 17 January 2019
Published online: 26 February 2019

References

1. Tollefson, J. Blue energy. *Nature* **508**, 302–304 (2014).
2. E. De Ranieri. Marine energy: In deep water. *Nature Energy*. **1**, 16007 (2016).
3. Oliveira, P., Taveira-Pinto, F., Morais, T. & Rosa-Santos, P. Experimental evaluation of the effect of wave focusing walls on the performance of the sea-wave slot-cone generator. *Energy Convers. Manag.* **110**, 165–175 (2016).
4. Wang, Z. L., Jiang, T. & Xu, L. Toward the blue energy dream by triboelectric nanogenerator networks. *Nano Energy* **39**, 9–23 (2017).
5. Xie, X. D., Wang, Q. & Wu, N. Energy harvesting from transverse ocean waves by a piezoelectric plate. *Int J. Eng. Sci.* **81**, 41–48 (2014).
6. Viet, N. V., Xie, X. D., Liew, K. M., Banthia, N. & Wang, Q. Energy harvesting from ocean waves by a floating energy harvester. *Energy* **112**, 1219–1226 (2016).
7. Wang, D. W., Mo, J. L., Wang, X. F., Ouyang, H. & Zhou, Z. R. Experimental and numerical investigations of the piezoelectric energy harvesting via friction-induced vibration. *Energy Convers. Manag.* **171**, 1134–1149 (2018).
8. Sun, S. & Tse, P. W. Design and performance of a multimodal vibration-based energy harvester model for machine rotational frequencies. *Appl. Phys. Lett.* **110**, 243902 (2017).
9. Shen, W., Zhu, S. & Zhu, H. Experimental study on using electromagnetic devices on bridge stay cables for simultaneous energy harvesting and vibration damping. *Smart Mater. Struct.* **25**, 065011 (2016).
10. Chen, J. et al. Micro-cable structured textile for simultaneously harvesting solar and mechanical energy. *Nat. Energy* **1**, 16138 (2016).
11. Donelan, J. M. et al. Biomechanical energy harvesting: generating electricity during walking with minimal user effort. *Science* **319**, 807–810 (2008).
12. Izadgoshasb, I. et al. Optimizing orientation of piezoelectric cantilever beam for harvesting energy from human walking. *Energy Convers. Manag.* **161**, 66–73 (2018).
13. Wang, W., Cao, J., Bowen, C. R., Zhou, S. & Lin, J. Optimum resistance analysis and experimental verification of nonlinear piezoelectric energy harvesting from human motions. *Energy* **118**, 221–230 (2017).
14. Elvin, N. G. & Elvin, A. A. Vibrational energy harvesting from human gait. *IEEE/ASME Trans. Mechatron.* **18**, 637–644 (2013).
15. Salauddin, M., Rasel, M. S., Kim, J. W. & Park, J. Y. Design and experiment of hybridized electromagnetic-triboelectric energy harvester using Halbach magnet array from handshaking vibration. *Energy Convers. Manag.* **153**, 1–11 (2017).
16. Zhang, F., Zang, Y., Huang, D., Di, C.-a & Zhu, D. Flexible and self-powered temperature-pressure dual-parameter sensors using microstructure-frame-supported organic thermoelectric materials. *Nat. Commun.* **6**, 8356 (2015).
17. Bai, X. et al. A magnetoelectric energy harvester with the magnetic coupling to enhance the output performance. *J. Appl. Phys.* **111**, 07A938 (2012).
18. Lin, Z. et al. Broadband and three-dimensional vibration energy harvesting by a non-linear magnetoelectric generator. *Appl. Phys. Lett.* **109**, 253903 (2016).
19. Mitcheson, P. D. et al. MEMS electrostatic micropower generator for low frequency operation. *Sens. Actuators A. Phys.* **115**, 523–529 (2004).
20. Wang, Z. L. & Song, J. H. Piezoelectric nanogenerators based on zinc oxide nanowire arrays. *Science* **312**, 242–246 (2006).
21. Jin, L. et al. Self-powered safety helmet based on hybridized nanogenerator for emergency. *ACS Nano* **10**, 7874–7881 (2016).
22. Yang, W. et al. Harvesting vibration energy by a triple-cantilever based triboelectric nanogenerator. *Nano Res.* **6**, 880–886 (2013).
23. Erturk, A., Hoffmann, J. & Inman, D. J. A piezomagnetoelastic structure for broadband vibration energy harvesting. *Appl. Phys. Lett.* **94**, 254102 (2009).
24. Deng, H. et al. A multimodal and multidirectional vibrational energy harvester using a double-branched beam. *Appl. Phys. Lett.* **112**, 213901 (2018).
25. Chen, J. & Wang, Z. L. Reviving Vibration energy harvesting and self-powered sensing by a triboelectric nanogenerator. *Joule* **1**, 480–521 (2017).
26. Deng, H. et al. A seesaw-type approach for enhancing nonlinear energy harvesting. *Appl. Phys. Lett.* **112**, 213902 (2018).
27. Yang, J. et al. Broadband vibrational energy harvesting based on a triboelectric nanogenerator. *Adv. Energy Mater.* **4**, 1301322 (2014).
28. Lan, C., Tang, L., Qin, W. & Xiong, L. Magnetically coupled dual-beam energy harvester: Benefit and trade-off. *J. Intel. Mat. Syst. Str.* **29**, 1216–1235 (2018).
29. Tang, L. & Yang, Y. A nonlinear piezoelectric energy harvester with magnetic oscillator. *Appl. Phys. Lett.* **101**, 094102 (2012).
30. Arrieta, A. F., Hagedorn, P., Erturk, A. & Inman, D. J. A piezoelectric bistable plate for nonlinear broadband energy harvesting. *Appl. Phys. Lett.* **97**, 104102 (2010).
31. Li, H., Dai, F. & Du, S. Broadband energy harvesting by exploiting nonlinear oscillations around the second vibration mode of a rectangular piezoelectric bistable laminate. *Smart Mater. Struct.* **24**, 045024 (2015).
32. Zou, H.-X. et al. Design and experimental investigation of a magnetically coupled vibration energy harvester using two inverted piezoelectric cantilever beams for rotational motion. *Energy Convers. Manag.* **148**, 1391–1398 (2017).
33. Syta, A., Bowen, C. R., Kim, H. A., Rysak, A. & Litak, G. Responses of bistable piezoelectric-composite energy harvester by means of recurrences. *Mech. Syst. Signal Pr.* **76-77**, 823–832 (2016).
34. Cao, J., Zhou, S., Wang, W. & Lin, J. Influence of potential well depth on nonlinear tristable energy harvesting. *Appl. Phys. Lett.* **106**, 173903 (2015).
35. Cottone, F., Gammaitoni, L., Vocca, H., Ferrari, M. & Ferrari, V. Piezoelectric buckled beams for random vibration energy harvesting. *Smart Mater. Struct.* **21**, 035021 (2012).
36. Ando, B., Baglio, S., Bulsara, A. R. & Marletta, V. A bistable buckled beam based approach for vibrational energy harvesting. *Sens Actuators A: Phys.* **211**, 153–161 (2014).
37. Cottone, F., Vocca, H. & Gammaitoni, L. Nonlinear energy harvesting. *Phys. Rev. Lett.* **102**, 080601 (2009).

38. Ferrari, M. et al. Improved energy harvesting from wideband vibrations by nonlinear piezoelectric converters. *Sens Actuators A: Phys.* **162**, 425–431 (2010).
39. Stanton, S. C., McGehee, C. C. & Mann, B. P. Nonlinear dynamics for broadband energy harvesting: Investigation of a bistable piezoelectric inertial generator. *Phys. D.* **239**, 640–653 (2010).
40. Kim, P. & Seok, J. A multi-stable energy harvester: dynamic modeling and bifurcation analysis. *J. Sound Vib.* **333**, 5525–5547 (2014).
41. Zhou, S., Cao, J., Erturk, A. & Lin, J. Enhanced broadband piezoelectric energy harvesting using rotatable magnets. *Appl. Phys. Lett.* **102**, 173901 (2013).
42. Oumbe Tekam, G. T., Kitio Kwuimy, C. A. & Woafo, P. Analysis of tristable energy harvesting system having fractional order viscoelastic material. *Chaos* **25**, 013112 (2015).
43. Zhou, Z., Qin, W. & Zhu, P. Improve efficiency of harvesting random energy by snap-through in a quad-stable harvester. *Sens Actuators A: Phys.* **243**, 151–158 (2016).
44. Zhou, Z., Qin, W. & Zhu, P. A broadband quad-stable energy harvester and its advantages over bi-stable harvester: Simulation and experiment verification. *Mech. Syst. Signal Pr.* **84**, 158–168 (2017).
45. Kim, P. & Seok, J. Dynamic and energetic characteristics of a tri-stable magnetopiezoelastic energy harvester. *Mech. Mach. Theory* **94**, 41–63 (2015).
46. Kim, P., Son, D. & Seok, J. Triple-well potential with a uniform depth: advantageous aspects in designing a multi-stable energy harvester. *Appl. Phys. Lett.* **108**, 243902 (2016).
47. Yung, K. W., Landecker, P. B. & Villani, D. D. An analytic solution for the force between two magnetic dipoles. *Magn. Electr. Sep.* **9**, 39–52 (1998).

Acknowledgements

The authors appreciate the support of the National Natural Science Foundation of China (grant nos. 11872167, 51575156, 51675156, 51775164, and 51705122), and the Fundamental Research Funds for the Central Universities (grant nos. JZ2017HGPA0165 and PA2017GDQT0024).

Author contributions

H.D. directed the scientific research of this work. H.D. and Y.D. conceived this idea and designed the prototype. Y.D. and Z.W. conducted the experiments and analyzed the data. H.D., Y.D., Z.W., J.Y., J.Z., M.M., and X.Z. discussed the results and commented on the paper together.

Additional information

Supplementary information accompanies this paper at https://doi.org/10.1038/s42005-019-0117-9.

Competing interests: The authors declare no competing interests.